J|A|C|S ARTICLES

Published on Web 02/17/2010

Size- and Site-Dependent Reconstruction in CdSe QDs Evidenced by ^{77}Se{^{1}H} CP-MAS NMR Spectroscopy

Derek D. Lovingood,[†] Randall Achey,[†] Anant K. Paravastu,[‡] and Geoffrey F. Strouse*,[†]

Department of Chemistry and Biochemistry, Florida State University, Tallahassee, Florida 32306-4390 and Department of Chemical and Biological Engineering, FAMU-FSU College of Engineering, Tallahassee, Florida 32310-6046

Received September 4, 2009; E-mail: strouse@chem.fsu.edu

Abstract: Evidence of size-dependent reconstruction in quantum dots leading to changes in bonding is observed through analysis of the ^{77}Se{^{1}H} cross-polarization magic angle spinning and ^{77}Se spin−echo solid-state NMR for Cd^{77}Se quantum dots. The CP-MAS and spin−echo data indicate discrete surface and core ^{77}Se sites exist with the QD, in which the surface is comprised of numerous reconstructed lattice planes. Due to the nearly 100% enrichment level for ^{77}Se, efficient spin coupling is observed between the surface ^{77}Se and sublayer ^{77}Se sites due to spin diffusion in the Cd^{77}Se quantum dots. The observed chemical shift for the discrete ^{77}Se sites can be correlated to the effective mass approximation via the Ramsey expression, indicating a $1/r^2$ size dependence for the change in chemical shift with size, while a plot of chemical shift versus the inverse band gap is linear. The correlation of NMR shift for the discrete sites allows a valence bond theory interpretation of the size-dependent changes in bonding character within the reconstructed QD. The NMR results provide a structural model for the QDs in which global reconstruction occurs below 4 nm in diameter, while an apparent self-limiting reconstruction process occurs above 4 nm.

Introduction

Semiconductor quantum dots (QDs), which are widely studied by optical spectroscopy, exhibit unique size-dependent properties that can be strongly influenced by reconstruction at the surface or in the core of the QD.[1−5] The exact nature of the reconstruction and the impact of surface ligation on reconstruction in a QD as a function of size are still controversial. Theoretical studies[6,7] on CdSe QDs have suggested reconstruction should occur in these materials due to surface strain. Analysis of the average QD structural environment by X-ray diffraction,[8] EXAFS/XANES,[9] and Rutherford back scattering[10,11] implies that overall QDs only experience minimal reconstruction that anneals out as the QD grows. More advanced studies have suggested a better model may require the inclusion of discrete sites (surface vs core) and a size-dependent behavior to fully interpret the impact of reconstruction in a QD.[7,12−20] A series of advanced studies on CdSe QDs using pair-distribution function analysis of X-ray data has probed the question of reconstruction to a greater degree and suggests reconstruction is localized at the nanocrystal surface, while the core of the nanocrystal is largely unperturbed.[12,13,15] Recent studies of the size-dependent elastic properties[14] have confirmed these findings but indicate CdSe below 3 nm exhibits a strongly perturbed structure potentially due to a change in the nature of reconstruction in the QD. Size-dependent analysis of CdSe QDs by pressure-dependent Raman measurements has also suggested a change in the Grüneisen parameter for CdSe QDs below 3

[†] Florida State University.
[‡] FAMU-FSU College of Engineering.

(1) Sachleben, J. R.; Wooten, E. W.; Emsley, L.; Pines, A.; Colvin, V. L.; Alivisatos, A. P. *Chem. Phys. Lett.* **1992**, *198*, 431–436.
(2) Tomaselli, M.; Yarger, J. L.; Bruchez, M.; Havlin, R. H.; deGraw, D.; Pines, A.; Alivisatos, A. P. *J. Chem. Phys.* **1999**, *110*, 8861–8864.
(3) Becerra, L. R.; Murray, C. B.; Griffin, R. G.; Bawendi, M. G. *J. Chem. Phys.* **1994**, *100*, 3297–3300.
(4) Jasieniak, J.; Mulvaney, P. *J. Am. Chem. Soc.* **2007**, *129*, 2841–2848.
(5) Sachleben, J.; Colvin, V.; Emsley, L.; Wooten, E. W.; Alivisatos, A. P. *J. Phys. Chem. B* **1998**, *102*, 10117–10128.
(6) Puzder, A.; Williamson, A. J.; Gygi, F.; Galli, G. *Phys. Rev. Lett.* **2004**, *92*, 4.
(7) Cherian, R.; Mahadevan, P. *Appl. Phys. Lett.* **2008**, *92*, 3.
(8) Bawendi, M. G.; Kortan, A. R.; Steigerwald, M. L.; Brus, L. E. *J. Chem. Phys.* **1989**, *91*, 7282–7290.
(9) Hamad, K. S.; Roth, R.; Rockenberger, J.; van Buuren, T.; Alivisatos, A. P. *Phys. Rev. Lett.* **1999**, *83*, 3474–3477.
(10) Schreuder, M. A.; McBride, J. R.; Dukes, A. D.; Sammons, J. A.; Rosenthal, S. J. *J. Phys. Chem. C* **2009**, *113*, 8169–8176.
(11) Kippeny, T. C.; Bowers, M. J.; Dukes, A. D.; McBride, J. R.; Orndorff, R. L.; Garrett, M. D.; Rosenthal, S. J. *J. Chem. Phys.* **2008**, *128*, 7.
(12) Neder, R. B.; Korsunskiy, V. I. *J. Phys.: Condens. Matter* **2005**, *17*, S125–S134.
(13) Gilbert, B.; Huang, F.; Zhang, H. Z.; Waychunas, G. A.; Banfield, J. F. *Science* **2004**, *305*, 651–654.
(14) Huxter, V. M.; Lee, A.; Lo, S. S.; Scholes, G. D. *Nano Lett.* **2009**, *9*, 405–409.
(15) Masadeh, A. S.; Bozin, E. S.; Farrow, C. L.; Paglia, G.; Juhas, P.; Billinge, S. J. L.; Karkamkar, A.; Kanatzidis, M. G. *Phys. Rev. B* **2007**, *76*, 11.
(16) Clark, S. M.; Prilliman, S. G.; Erdonmez, C. K.; Alivisatos, A. P. *Nanotechnology* **2005**, *16*, 2813–2818.
(17) Gilbert, B.; Zhang, H.; Chen, B.; Kunz, M.; Huang, F.; Banfield, J. F. *Phys. Rev. B* **2006**, *74*, 7.
(18) Chen, B.; Penwell, D.; Benedetti, L. R.; Jeanloz, R.; Kruger, M. B. *Phys. Rev. B* **2002**, *66*, 4.
(19) Cerullo, G.; De Silvestri, S.; Banin, U. *Phys. Rev. B* **1999**, *60*, 1928–1932.
(20) Ithurria, S.; Guyot-Sionnest, P.; Mahler, B.; Dubertret, B. *Phys. Rev. Lett.* **2007**, *99*, 4.

 10.1021/ja907511r

nm.[21,22] While these techniques have provided insight into the overall changes in the structure as a function of size, the use of an analytical technique that is selective for select elements within the lattice and specific to the location of these elemental sites would be ideal to address the nature of bonding and reconstruction experienced by a QD.

Due to the element specificity inherent to nuclear magnetic resonance (NMR) methods, ease of synthesis, and well-studied properties for CdSe,[23,24] this manuscript analyzes the size-dependent reconstruction on ^{77}Se-enriched CdSe QDs (Cd^{77}Se) using NMR methods to structurally depth profile specific ^{77}Se atoms in local chemical environments. Solid-state NMR studies of Cd^{77}Se QDs, ranging in size from 2 to 7 nm, with a 5−6% size dispersity are analyzed allowing discrete assignment of the core, surface, and passivant ^{77}Se sites within the QD as well as evidence of size-dependent QD reconstruction. Of the NMR active species in a CdSe QD (^{113}Cd, ^{77}Se, ^{13}C, ^{31}P, and ^{1}H),[3,5,25−32] the ^{77}Se atom (spin 1/2) is convenient to study because of the environmental sensitivity of its chemical shift[32] and the ability to isotopically enrich the element. For the Cd^{77}Se QD samples, the NMR chemical shifts as a function of size reveal that the ligation layer is unique and apparently uncoupled to QD size effects, while the surface (outermost shells) and core (innermost shells) environments exhibit different magnitudes of reconstruction depending on the size of the QD. As the QD grows above 4 nm in diameter, reconstruction appears to be more localized to surface layers while the core appears to be largely unperturbed. Since semiconductor QDs and more importantly CdSe are being applied in a diverse range of technologies, understanding the structural attributes of reconstruction and the impact on the outermost planes relative to the core of the QD is crucial.

NMR methods can allow the differentiation of discrete chemical environments within a QD by analyzing the chemical shift of the elemental sites and discriminating the elemental signal associated with a surface versus a core of a QD.[1−3,5,25,26,30−44] Cross-polarization magic angle spinning (CP-MAS) can allow the surface versus core signals to be delineated, since CP enhancement is a heteronuclear short-range process[25,26,32,38] dependent on numbers of nuclei, relative geometries, and the Hartmann−Hahn matching condition.[2,32,34,45,46] Spin−echo measurements allow a more global analysis of the lattice properties, and by coupling spin−echo and CP experiments, it is possible to delineate the NMR contributions from the surface and sublayers in the QD. Although there could be multiple ^{1}H populations influencing the CP signals (which are face, site, and passivant density specific), the passivant ^{1}H nuclei nearest the surface layer will dominate the polarization transfer process. Carr−Purcell−Meiboom−Gill (CPMG) NMR acquisitions increase NMR sensitivity for these samples without significant distortion of the ^{77}Se line shape, allowing ^{77}Se T_1 (spin−lattice) and T_2 (spin−spin) relaxation measurements for the QD. Interpretation of the NMR data is a powerful analytical tool for structural analysis in QDs but is limited by the broadening of NMR features due to disorder in nanoscale materials with high surface-to-core ratios.[32,44]

Isotopic enrichment of the ^{77}Se sites enhances spin diffusivities, facilitating assignment of ^{77}Se signals to different layers within the QD through analysis of the variable CP contact times. NMR chemical shifts as a function of size reveal that the ligation layer is unique and apparently uncoupled to QD size effects, while the surface (outermost shells) and core (innermost shells) environments exhibit different magnitudes of reconstruction depending on the size of the QD. On the basis of chemical shift analysis as a function of CP times, global reconstruction is observed for QDs below 4 nm while the reconstruction appears to be self-limited for QDs greater than 4 nm. As the QDs change size, reconstruction appears to be more localized to surface layers while the core appears to be largely unperturbed. Surface reconstruction appears to influence the effectiveness of spin diffusion between QD surface and core regions, which could have implications to NMR studies across semiconductor nanostructure interfaces.[47,48] The T_1 and T_2 results show a discontinuity around 4 nm, which may imply the largest change in reconstruction occurs in this size regime. Analysis of the chemical shifts using the Ramsey expression coupled to valence bond theory provides insight into the changes in local bonding that occur with size and indicates the surface sites have greater *s* character for the Cd−Se bonds due to compressive strain. The change in bonding is consistent with the expectation for passivant chelation and surface dangling bonds in a QD. The NMR-based model for Cd^{77}Se reconstruction supports the

(21) Meulenberg, R. W.; Strouse, G. F. *J. Phys. Chem. B* **2001**, *105*, 7438–7445.
(22) Meulenberg, R. W.; Jennings, T.; Strouse, G. F. *Phys. Rev. B* **2004**, *70*, 5.
(23) Murray, C. B.; Kagan, C. R.; Bawendi, M. G. *Science* **1995**, *270*, 1335–1338.
(24) Colvin, V. L.; Schlamp, M. C.; Alivisatos, A. P. *Nature* **1994**, *370*, 354–357.
(25) Wang, R.; Calvignanello, O.; Ratcliffe, C. I.; Wu, X.; Leek, D. M.; Zaman, M. B.; Kingston, D.; Ripmeester, J. A.; Yu, K. *J. Phys. Chem. C* **2009**, *113*, 3402–3408.
(26) Ratcliffe, C. I.; Yu, K.; Ripmeester, J. A.; Zaman, M. B.; Badarau, C.; Singh, S. *Phys. Chem. Chem. Phys.* **2006**, *8*, 3510–3519.
(27) M. Kuno, J. K. L.; Dabbousi, B. O.; Mikulec, F. V.; Bawendi, M. G. *J. Chem. Phys.* **1997**, *106*, 9869–9882.
(28) Liu, H.; Owen, J. S.; Alivisatos, A. P. *J. Am. Chem. Soc.* **2007**, *129*, 305–312.
(29) Kopping, J. T.; Patten, T. E. *J. Am. Chem. Soc.* **2008**, *130*, 5689–5698.
(30) Mikulec, F. V.; Kuno, M.; Bennati, M.; Hall, D. A.; Griffin, R. G.; Bawendi, M. G. *J. Am. Chem. Soc.* **2000**, *122*, 2532–2540.
(31) Thayer, A. M.; Steigerwald, M. L.; Duncan, T. M.; Douglass, D. C. *Phys. Rev. Lett.* **1988**, *60*, 2673–2676.
(32) Berrettini, M. G.; Braun, G.; Hu, J. G.; Strouse, G. F. *J. Am. Chem. Soc.* **2004**, *126*, 7063–7070.
(33) Watanabe, S.; Sasaki, S. *Jpn. J. Appl. Phys., Part 2: Lett.* **2003**, *42*, L1350–L1352.
(34) V. Ladizhansky, G. H.; Vega, S. *J. Phys. Chem. B* **1998**, *102*, 8505–8509.
(35) Pines, A.; Gibby, M. G.; Waugh, J. S. *J. Chem. Phys.* **1973**, *59*, 569–590.
(36) Panich, A. M.; Sergeev, N. A.; Shlimak, I. *Phys. Rev. B* **2007**, *76*, 8.
(37) M. Gavish, S. V.; Zamir, D. *Phys. Rev. B* **1993**, *48*, 2191–2199.
(38) Lo, A. Y. H.; Sudarsan, V.; Sivakumar, S.; van Veggel, F.; Schurko, R. W. *J. Am. Chem. Soc.* **2007**, *129*, 4687–4700.
(39) Ladd, T. D.; Maryenko, D.; Yamamoto, Y.; Abe, E.; Itoh, K. M. *Phys. Rev. B* **2005**, *71*, 12.
(40) Huang, Y. N.; Yan, Z. M. *J. Am. Chem. Soc.* **2005**, *127*, 2731–2740.
(41) Franzoni, M. B.; Levstein, P. R. *Phys. Rev. B* **2008**, *78*, 5.
(42) Franzoni, M. B.; Levstein, P. R. *Phys. Rev. B* **2005**, *72*, 5.
(43) Dementyev, A. E.; Li, D.; MacLean, K.; Barrett, S. E. *Phys. Rev. B* **2003**, *68*, 4.
(44) Cadars, S.; Smith, B. J.; Epping, J. D.; Acharya, S.; Belman, N.; Golan, Y.; Chmelka, B. F. *Phys. Rev. Lett.* **2009**, *103*, 136802.
(45) Hartmann, S. R.; Hahn, E. L. *Phys. Rev.* **1962**, *128*, 2042–&.
(46) R. Elbaum, S. V.; Hodes, G. *Chem. Mater.* **2001**, *13*, 2272–2280.
(47) Tycko, R.; Barrett, S. E.; Dabbagh, G.; Pfeiffer, L. N.; West, K. W. *Science* **1995**, *268*, 1460–1463.
(48) Goehring, L.; Michal, C. A. *J. Chem. Phys.* **2003**, *119*, 10325–10329.

findings of Billinge et al.[15] and Scholes et al.,[14] who postulate size-dependent reconstruction.

Experimental Section

Chemicals. Cadmium stearate (CdSA) (90%, Strem Chemical), 1-octadecene (ODE) (90%, Sigma Aldrich), selenium powder (99.66% enriched ^{77}Se, Isoflex USA), and tri-*n*-octylphosphine (TOP) (90%, Alfa Aesar) were used without further purification.

Synthesis of Cd^{77}Se QDs from Cadmium Stearate (CdSA). Cd^{77}Se QDs were grown by lyothermal methods using a modified literature reaction involving CdSA and TOP−^{77}Se.[49] CdSA was added to 1-octadecene in a 3-neck round-bottom flask under N_2 and degassed according to the literature procedures. The reaction mixture was heated. TOP−^{77}Se was injected and allowed to stir until the target QD size was obtained; size was monitored by UV−Vis absorption of aliquots. The reaction temperatures used were 180 (3.1 nm), 280 (4.32 nm), and 300 (6.1 and 6.9 nm) °C for each targeted QD size. The reaction was allowed to cool to room temperature and the QD isolated by centrifugation through standard selective precipitation methods via the addition of *n*-butanol to the reaction mixture followed by toluene/methanol dissolution/precipitation steps. The samples were dried under vacuum at room temperature, and the solid powdered samples were packed into 2.5 mm zirconia Varian NMR rotors.

Synthesis of Cd^{77}Se QD from Li$_4$[Cd$_{10}$^{77}Se$_4$(SePh)$_{16}$]. For comparison a Cd^{77}Se QD lacking an ^{77}Se-enriched passivant layer was prepared as the smallest QD (2.9 nm) via a single-source precursor route[50] using Li$_4$[Cd$_{10}$^{77}Se$_4$(SePh)$_{16}$] grown in the presence of hexadecylamine at 230 °C. The actual enrichment level of the core and surface of the 2.9 nm QD will be less than 100%, as it is known that selenophenol (SePh) will decompose during the reaction and act as a Se donor atom during QD growth.[50,51] Thus, the passivant layer will consist of a SePh (unenriched Se) and TOP/TOPO following ligand exchange. Once the reaction was at the desired QD size, the reaction was allowed to cool to room temperature and the QD isolated by centrifugation through standard selective precipitation methods using toluene/methanol dissolution/precipitation steps. The sample was dried under vacuum at room temperature, and the solid powdered sample was packed into 2.5 mm zirconia Varian NMR rotors.

Instrumentation. Solid-State Nuclear Magnetic Resonance. All solid-state NMR experiments were performed on a Varian Unity/Inova 11.75 T spectrometer with a Chemagnetics triple-resonance 2.5 mm broad-band magic angle spinning (MAS) probe using zirconia rotors. The probe was tuned to 500.1 MHz for ^{1}H and 95.36 MHz for ^{77}Se; the third channel was not used in this study. An MAS speed of 12 kHz was used in all experiments, except some ^{1}H $T_{1\rho H}$ experiments conducted at 24 kHz MAS. The ^{77}Se chemical shifts were determined relative to an external reference standard of dimethyl selenide, $Se(CH_3)_2$, at 0 ppm. Multiple ^{77}Se experiments were run on the samples including ^{77}Se{^{1}H} CP-MAS, ^{77}Se spin−echo, and ^{77}Se saturation recovery CPMG.

CP-MAS. ^{77}Se{^{1}H} CP-MAS spectra were acquired using ^{1}H decoupling, ramped cross-polarization (CP), an acquisition time of 5 ms, a recycling delay of 3 s, and a 90° pulse length of 5 μs. The contact time was varied (1−40 ms), allowing different polarization transfer times between the ^{1}H and ^{77}Se nuclei. Least-squared fits of CP-MAS NMR spectra to multiple Gaussian line-shape components were accomplished using Mathematica. During the initial fitting the amplitude, fwhm, and chemical shift position were allowed to float on the 12 or 15 ms contact time point. This time point was chosen because contributions for the core and surface were readily observable. Once the fundamental resonances were identified the other time points were fit keeping the fwhm and chemical shift position constant and allowing only the amplitude to be varied. CP-MAS buildup data were constructed from integrated area verses contact time and fit to the following equation

$$M(\tau) = \frac{M_0\left[\exp\left(\frac{-\tau}{T^*_{1\rho H}}\right) - \exp\left(\frac{-\tau}{T^*_{HSe}}\right)\right]}{1 - \frac{T^*_{HSe}}{T^*_{1\rho H}}} \quad (1)$$

The validity of assumptions underlining the derivation of eq 1 are discussed later in the text.

Spin−Echo. ^{77}Se spin−echo spectra were performed with an acquisition time of 1.5 ms, a recycling delay of 180 s, and a 90° and 180° pulse length of 3.25 and 6.50 μs, respectively. Least-squared fits for the spin−echo NMR spectra were accomplished in Mathematica with the total number of peaks for each spectrum kept to a minimum. Spin−echo pulse methods were chosen to measure the overall Se environments in the QDs in order to avoid loss of signal-to-noise due to ring down.

Saturation Recovery−CPMG. ^{77}Se spin−lattice relaxation (T_1) times and spin−spin relaxation (T_2) times were determined by using a saturation recovery−CPMG pulse sequence. The parameters used for these experiments include a recycle delay of 1 s, a 90° and 180° pulse length of 3.25 and 6.5 μs, 20 saturation 90° pulses ($_N$Sat) separated by 50 μs, and 1000 echo pulses ($_N$Echo) separated by 1 ms. Delay between saturation and acquisition was varied from 0.1 ms to 4320 s depending on the sample. The aturation recovery−CPMG pulse sequence can be found in the Supporting Information (Supporting Information Figure 1). Comparison of the total integrated signal area vs relaxation delay allows for T_1 of the overall QD to be calculated. Analysis of the FID decay of each echo train allows for the T_2 of the overall QD to be determined. T_1 and T_2 were calculated for the Cd^{77}Se samples using the following expressions

$$y(\tau) = A \times \left[1 - \exp\left(\frac{-\tau}{T_1}\right)\right] \quad (2)$$

$$y(\tau) = A_1 \times \left[1 - \exp\left(\frac{-\tau}{T_{2,1}}\right)\right] + A_2 \times \left[1 - \exp\left(\frac{-\tau}{T_{2,2}}\right)\right] \quad (3)$$

where $T_{2,1}$ and $T_{2,2}$ represent biexponential time constants for T_2 decay.[33,36,38,39,41,52] Supporting Information Figure 2 shows ^{77}Se spin−echo and ^{77}Se CPMG spectra for the 3.1 and 6.9 nm Cd^{77}Se overlaid on top of each. This shows the consistency between the experiments and that ^{1}H was not needed during the measurements.

^{1}H Spin Lock. ^{1}H $T_{1\rho H}$ relaxations were measured using a spin lock pulse sequence with an acquisition time of 5 ms, recycle delay of 3 s, 90° pulse length of 5 μs, and a spinning speed of 12 and 24 kHz. The spin lock time was varied from 5 to 145 ms.

UV−Vis. Optical absorption was analyzed in a 1 cm cell in toluene ($\sim 1 \times 10^6$ mol) using a Cary 50 UV−vis spectrophotometer. The absorption maxima for the first exciton was used to estimate the QD size during the reaction to form the QD.[23]

Powder X-ray Diffraction. Powder X-ray diffraction (pXRD) was carried out on a Rigaku DMAX 300 Ultima 3 diffractometer using Cu Kα ($\lambda = 1.5418$ A) with the *d* spacing calibrated to a Si_0 standard to verify crystal motif. Using the Debye−Scherrer[50] formula the QD diameter was calculated using the ⟨110⟩ peak, which helps eliminate complications from overlapping reflections.

Transmission Electron Microscopy (TEM). QD size, dispersity, and morphology were analyzed by TEM using a JEOL-2010

(49) A. L. Washington, I.; Strouse, G. F. *J. Am. Chem. Soc.* **2008**, *130*, 8916–8922.
(50) Lovingood, D. D.; Oyler, R. E.; Strouse, G. F. *J. Am. Chem. Soc.* **2008**, *130*, 17004–17011.
(51) Archer, P. I.; Santangelo, S. A.; Gamelin, D. R. *J. Am. Chem. Soc.* **2007**, *129*, 9808–9818.
(52) Li, D.; Dong, Y. Q.; Ramos, R. G.; Murray, J. D.; MacLean, K.; Dementyev, A. E.; Barrett, S. E. *Phys. Rev. B* **2008**, *77*, 26.

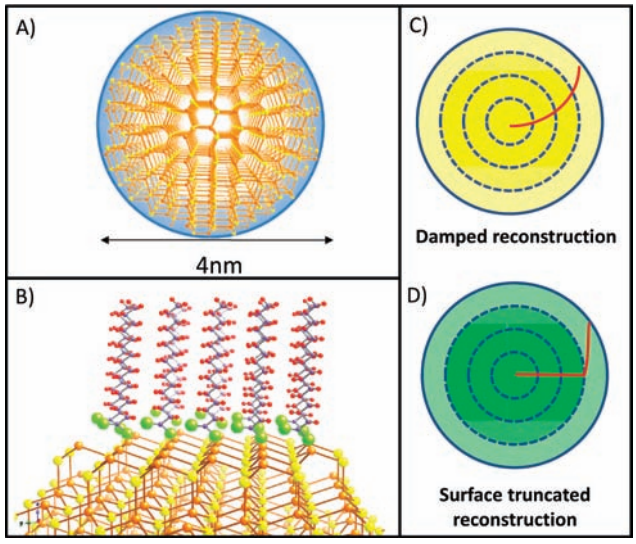

Figure 1. (A) Drawing of a 4 nm, truncated wurtzite CdSe QD highlighting the distinctive regions within the QD representing the surface ligation layer (dark blue), near surface layers (light blue), and core layers (white). (B) Ligand passivation layer on the ⟨101⟩ plane of a CdSe QD. (C and D) Possible reconstruction models where lattice reconstruction induced by surface ligation is (C) weakly or (D) strongly damped by the within the lattice planes.

microscope operated at 200 kV. The QDs were dispersed on holey carbon (400 mesh) from a toluene solution. Size dispersities were measured by averaging ∼100 individual dots from the TEM.

X-ray Fluorescence. Elemental composition analysis for Cd^{2+} and Se^{2-} was carried out in an Oxford Instruments ED_{2000} X-ray fluorescence spectrometer with a Cu Kα source. The Cd^{2+} to Se^{2-} mole ratio was determined for each sample by running four repeat analyses to minimize statistical error. For a standard XRF measurement, the powdered samples were completely dissolved in 90% HNO_3, heated to remove excess NO_x, and then diluted to ∼3 mL with a 2% HNO_3 solution (to allow compatibility with the XRF sample holder). All measurements were carried out using the Kα line for Cd^{2+}(23.1 keV) and Se^{2-} (11.2 keV). Calibration curves were generated using commercially prepared 1000 ppm elemental standards in 2% HNO_3, which results in accuracies of 3 ppm for Cd^{2+} and 4 ppm for Se^{2-}.

Results/Discussion

From a simplistic viewpoint, a QD can be envisioned as a fragment of a larger bulk crystalline lattice consisting of a series of shells in which the outermost layer is truncated along high-energy lattice planes. The presence of surface passivants in the surface ligation layer can alter the bonding interactions in the QD, potentially causing both the surface and the core to relax to minimize strain. Surface reconstruction in bulk materials is a common phenomenon that lowers the potential energy of dangling bonds and can result in strong perturbation of the chemical potential over multiple layers.[53] In Figure 1A, a simplified representation of the different potential environments experienced by a Se atom in CdSe can be defined, such that one can visualize a passivation layer dominated by the surface-to-ligand interaction (dark blue), a surface layer that is perturbed by the chemical potential of the ligation layer (light blue), and a core (white) that resembles the bulk chemical environment. If we consider the QD surface ligation layer (Figure 1B), dangling bonds due to unpassivated sites and ligation of the Cd (or Se) sites by a passivating ligand such as trioctylphosphine will lower the local symmetry as well as change the chemical environment of those sites. Whether these local changes in chemical potential are represented as a gradient with complete global reconstruction (Figure 1C) or rapidly damped resulting in *only* the outermost layers being reconstructed (Figure 1D) will be strongly dependent on the material type, QD size, and nature of the passivant. Literature reports suggest either model may be applicable depending on the QD.[13−15]

Analysis of Passivating Layer, Surface, and Core. Spherical $Cd^{77}Se$ QDs passivated by stearic acid and TOP−^{77}Se in the size range 3.1−6.9 nm exhibiting a wurtzite morphology with 5−6% size dispersity were prepared by standard lyothermal growth methods using cadmium stearate and TOP−^{77}Se, and for comparison a 2.9 nm QD was grown without TOP−^{77}Se via a single-source precursor route[50] using $Li_4[Cd_{10}{}^{77}Se_4(SePh)_{16}]$. Characterization data (absorption, TEM, and pXRD) for the individual QD samples are available in Supporting Information Figure 3. The results of ^{77}Se{^{1}H} CP-MAS and spin−echo NMR measurements on wurtzite $Cd^{77}Se$ QDs are summarized in Table 1, which reports the chemical shifts of line-shape components observed in the NMR spectra. Peak intensities are not tabulated in Table 1 because they are not necessarily indicative of the number of spins in the different reservoirs.

The size-dependent ^{77}Se{^{1}H} CP-MAS NMR measurements of $Cd^{77}Se$ at multiple polarization times are shown in Figure 2. The CP-MAS NMR profiles exhibit both size and CP contact time-dependent changes between 0 and −1000 ppm. The changes in the CP-MAS NMR profiles with contact time will be complex due to potential contributions from ligation layer influences of cross-polarization dynamics and changes in spin diffusion with size between the surface and core sublayers. Isotopic enrichment (99.7%) of ^{77}Se is expected to dramatically increase ^{77}Se spin diffusion rates in these samples. It is reasonable to expect that at short contact times (1−4 ms) the surface Se sites should be more efficiently polarized via direct ^{1}H−^{77}Se dipolar couplings, at intermediate contact times (8−15 ms) a mixture of surface and core Se sites will polarize due to spin diffusion through the ^{77}Se lattice, and at longer contact times (>22 ms) the core Se sites will be the dominant contributors through spin diffusion to the largest spin reservoir.

In Figure 2, the individual NMR features exhibit different spectral line-width and contact time-dependent intensities consisting of two reasonably sharp features and a broad feature (only one sharp feature and one broad feature were considered in line-shape fits for the 2.9 nm QD). Inspection of the ^{77}Se NMR features in Figure 2 reveals all ^{77}Se signals have a more negative chemical shift in comparison to ^{77}Se in bulk CdSe. Since the efficiency of cross-polarization drops rapidly with the distance, the CP-MAS NMR resonances between −479 and −512 ppm (peak 1 in Table 1) observed to be most intense at the longest polarization times suggest these ^{77}Se NMR signatures must arise furthest from the ligation layer and thus are assigned to core ^{77}Se sites (at least 2−3 lattice planes down). The broad feature (−500 to −590 ppm; peak 2) and the sharpest feature (ca. −600 ppm; TOP−^{77}Se peak, labeled with an asterisk in Figure 2) in the CP-MAS data are most intense at the shortest polarization times and thus likely reflect contributions from Se atoms at or near the passivation layer on the QD due to the short-range efficiency of CP methods. The TOP−^{77}Se feature (asterisk in Figure 2) is assigned to the passivation of the QD due to the absence of the feature in the NMR for the 2.9 nm

(53) Duke, C. B. *Chem. Rev.* **1996**, *96*, 1237–1259.

Table 1. Summary of Data

	$Li_4[Cd_{10}{}^{77}Se_4(SePh)_{16}]$	sample 1	sample 2	sample 3	sample 4	sample 5	bulk	TOP−^{77}Se
peak abs		521.0	554.6	595.1	626.4	646.9		
$size_{XRD}$ (nm)		2.95		4.32	6.14	6.70		
$size_{TEM}$ (nm)			3.08 ± 0.17	4.36 ± 0.05	6.15 ± 0.46	6.90 ± 0.49		
total atoms		483	540	1528	4350	6199		
no. of lattice planes in *a*,*b*/*c*		4/7	4/8	6/11	8/16	10/18		
XRF-Cd:Se	1:2.12	1:1.08	1:0.9	1:0.95	1:1.03	1:1.05	1:1.03	
^{77}Se T_1 (s)		270.7 ± 24.0	238.0 ± 27.3	163.1 ± 5.6	286.2 ± 7.8	209.7 ± 7.0	1667 ± 181	0.73 ± 0.06
^{77}Se $T_{2,1}$ (ms)		61.3 ± 4.2	52.4 ± 8.9	37.1 ± 4.5	17.3 ± 1.1	16.6 ± 0.6	410.6 ± 57.9	198.1 ± 16.1
^{77}Se $T_{2,2}$ (ms)		3.1 ± 0.1	3.7 ± 1.1	11.1 ± 3.2	4.4 ± 0.7	2.5 ± 0.4	24.0 ± 2.0	
			^{77}Se spin−echo					
peak 1 (ppm)	−650.7	−499.1	−500.9	−493.0	−480.8	−478.1	−472.3	−389.0
peak 2 (ppm)	−697.5	540.8	−524.5	−543.8	−483.9	−479.1		−396.6
TOP−^{77}Se* (ppm)			−600.3					
			^{1}H−^{77}Se CP-MAS					
peak 1 (ppm)		−512.6	−501.2	−494.3	−485.8	−479.5		
peak 2 (ppm)		−520.8	−589.3	−569.3	−551.7	−500.6		
TOP−^{77}Se* (ppm)			−602.4	−600.7	−601.6	−613.4		

CdSe QD grown in the absence of TOP−^{77}Se (Figure 2A). Furthermore, the assignment for TOP−^{77}Se is consistent with the predicted NMR shift if one considers the relative electronegativities of selenium and phosphorus (2.55 and 2.19, respectively), which would result in increased shielding of ^{77}Se sites bound to TOP due to the increased electron density on the more electronegative Se atom. Finally, the assumption that the sharpest feature is TOP−^{77}Se is also consistent with the greater rotational and translational freedom for the ligand.

The chemical shifts for peaks 1 and 2 are QD size dependent, and therefore, it is reasonable to assume the ^{77}Se sites are assignable to lattice sites within the QD. The broader line width for peak 2 with respect to peak 1 may reflect a distribution in the chemical environments for these near-surface ^{77}Se sites. The chemical shift for the TOP−^{77}Se peak (asterisk in Figure 2) does not show a QD size dependence as expected for nuclei that have minimal interaction with the QD lattice. The validity of the assignments from CP-MAS are supported by the spin−echo NMR for the bulk-like and surface-like features (Figure 3A). The assignments of the core and surface sites for Se in Cd^{77}Se are consistent with earlier reports.[31,32]

Comparing CP-MAS data to spin−echo measurements provides further insight into the spectral features observed in NMR, since spin−echo is a more quantitative representation of different ^{77}Se populations. For both CP-MAS and spin−echo measurements, a decrease in the NMR intensity for the surface ^{77}Se (relative to the core sites) is observed with increasing QD size (Figures 2 and 3A) as expected for the decreasing surface to volume ratio as the QD grows. The observation can thus be correlated with the number of atoms in the lattice planes of the QDs by plotting the percentage of the core and surface for a theoretical QD and for the integrated area for the NMR signals as a function of QD size (Figure 3). The contributions of the core and surface NMR signals from spin−echo (Figure 3A) appear to follow a size-dependent trend between 4.3 and 6.9 nm, while the ∼3 nm QDs do not follow the observed trend. The trend for QDs larger than 4 nm can be understood by considering the regions described in Figure 1A where a surface can be defined within 2 Å (∼1 lattice plane, solid line) or 3.25 Å (∼2 lattice planes, dashed line). Details of the calculation are available in the Supporting Information. If we consider a projection along the ⟨002⟩ plane for a wurtzite CdSe QD, this

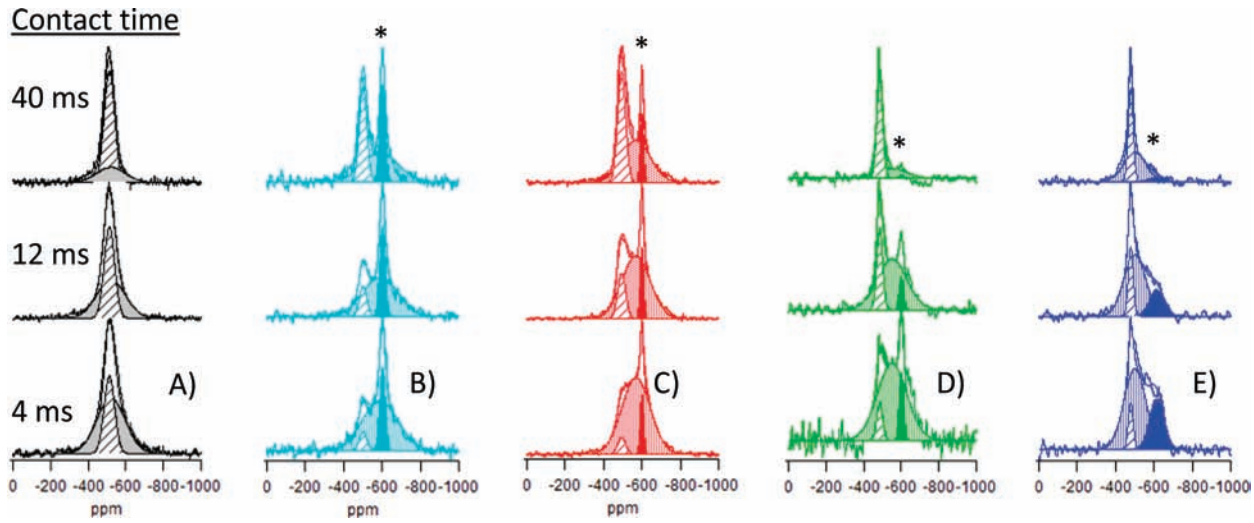

Figure 2. ^{77}Se{^{1}H} CP-MAS NMR at 4, 12, and 40 ms contact times for Cd^{77}Se QDs: (A) 2.9 (black), (B) 3.1 (light blue), (C) 4.3 (red), (D) 6.1 (green), and (E) 6.9 nm (dark blue). Fits are assigned as follows: peak 1 (slashed) core ^{77}Se sites; peak 2 (dotted) near-surface and surface ^{77}Se sites; and peak 3 (solid) surface ^{77}Se site bound to a TOP ligand. The peak labeled with an asterisk (*) identifies the NMR resonance associated with a surface-bound TOP through a ^{77}Se on the QD surface. The overall fit of the deconvuluted spectra has been added to each spectrum.

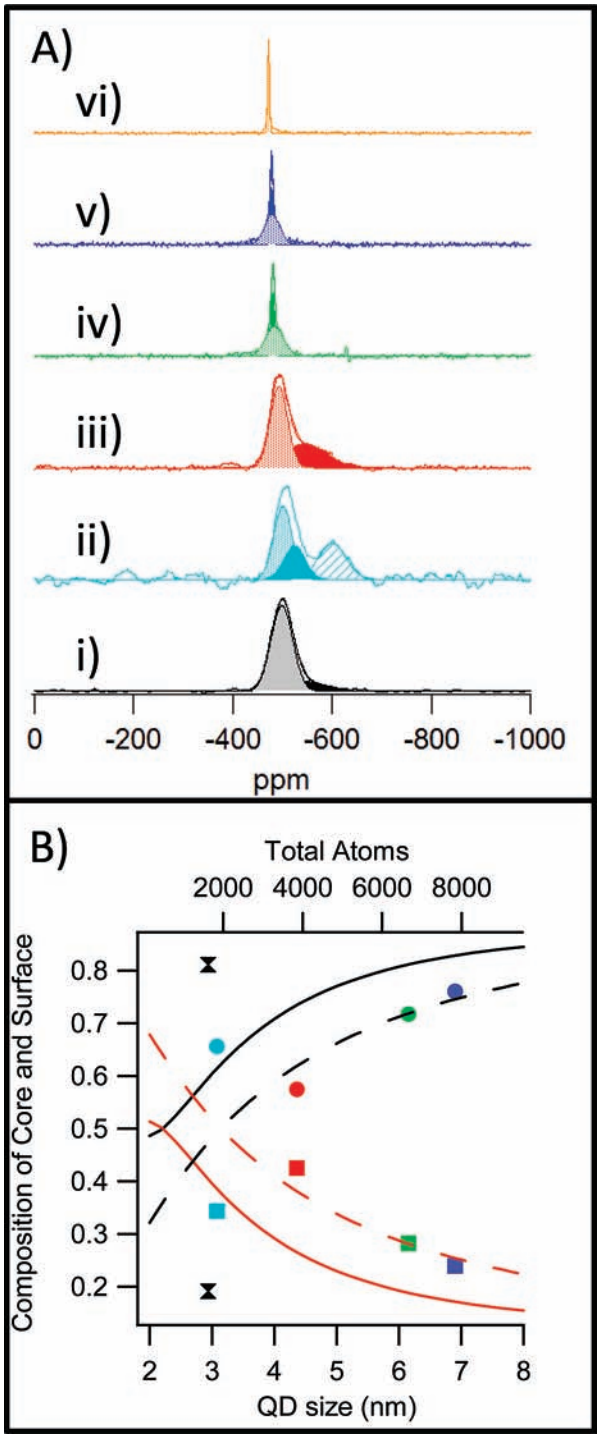

Figure 3. (A) Spin−echo (i−v) and direct pulse (vi) NMR of (i) 2.9 (black), (ii) 3.1 (light blue), (iii) 4.3 (red), (iv) 6.1 (green), (v) 6.9 (dark blue), and (vi) bulk CdSe (orange). (B) Size-dependent changes in the composition of surface and core assuming T_1 and T_2 are similar for the regions. Circles represent core signal and squares represent surface signals. The hourglass represents the smallest QD grown from cluster.

observation would suggest that the assigned fits for the surface contain surface and near surface Se atoms within the suggested 2 lattice planes while the core Se resonances arise from the remaining $n-2$ lattice planes; n is the number of lattice planes.

Although the finding of significant changes occurring below 4 nm is in good agreement with experimental observations that QDs below 4 nm are structurally different,[14,15,22] it is possible the failure to follow the surface to core trend lines in Figure 3B for QDs below 4 nm may reflect the low number of definable lattice planes for a QD of this size, lattice disorder arising from twinning or cubic inclusions in the wurtzite lattice,[8] or potentially a mixture of wurtzite and zinc-blende structures within the Cd^{77}Se QD sample.[15] All these phenomena would result in local variations to atom density and the inability to follow a theoretical plot based on a pure wurtzite structure. Whether the assignment of definitive core and surface contributions reflect disorder or reconstruction is unclear; however, the observation of discrete core and surface NMR signatures that correlate with the number of lattice planes and the size of the QD suggests significant reconstruction occurs over several layers while the core sites experience a smaller degree of reconstruction for QDs bigger than 4 nm in diameter (Figure 1D).

Site-Dependent CP Buildup Curves. Although the data in Figure 4 fit well to the canonical CP buildup equation (eq 1),[54] this equation was derived with limiting assumptions that are not appropriate to the present samples. For a 100% enriched sample the (i) ^{77}Se is not low in abundance relative to ^{1}H because of its isotopic enrichment[54] and (ii) homonuclear dipolar coupling allows signal enhancement of ^{77}Se sublayer atoms that are not directly coupled to ^{1}H. The breakdown of assumption (i) can result in an increase of the observed time constants relative to the values expected in the limit of low ^{77}Se abundance.[40,54−57] To properly describe the CP data in Figure 4 and Table 2, ^{77}Se spin diffusion from the cross-polarized surface into the bulk of the QD must be considered, and thus, in the manuscript we use the superscript asterisk to emphasize that T^*_{HSe} and $T^*_{1\rho H}$ are phenomenological parameters that are affected by the non-negligible population of the ^{77}Se reservoir and by ^{77}Se spin diffusion.

The best-fit time constants, T^*_{HSe} and $T^*_{1\rho H}$, for core, surface, and TOP-bound ^{77}Se as a function of Cd^{77}Se QD size are summarized in Table 2. For the two smallest QD samples (3.1 and 4.3 nm), the TOP−^{77}Se layer exhibits a longer T^*_{HSe} than the surface QD layer. This result suggests differential importance of ligand binding on different QD surfaces; in other words, the surface Cd^{77}Se layer is most strongly coupled to a subset of the overall TOP−^{77}Se. Comparing the data for the TOP−^{77}Se layers for different QD sizes, an apparent discontinuity is observed between the small samples (3.1 and 4.3 nm) and the larger samples (6.1 and 6.9 nm). This observation could suggest an abrupt size-dependent change in the passivant layer as previously reported.[21] Repeated measurements confirm the values in Table 2, suggesting that the results are not experimental artifacts.

The origin of the anomalies observed for the surface T^*_{HSe} and $T^*_{1\rho H}$ in the 6.1 nm Cd^{77}Se and the $T_{1\rho H}$ observed in the 4.3 nm Cd^{77}Se is unclear. A possible explanation for the behavior at 6.1 nm could concern the formation of a stable crystalline facet which has been observed to change the apparent ligand packing for CdSe above 4.5 nm.[21] Although the frequency of the assigned ^{77}Se resonance for the TOP−^{77}Se in the CP-MAS data shows no discernible shift with QD size, the 4.3 nm Cd^{77}Se QD data exhibit a directly detected $T_{1\rho H}$ that is smaller than the analogous value extracted by CP-MAS. This

(54) Kolodziejski, W.; Klinowski, J. *Chem. Rev.* **2002**, *102*, 613–628.
(55) Ando, S.; Harris, R. K.; Reinsberg, S. A. *J. Magn. Reson.* **1999**, *141*, 91–103.
(56) Ando, S.; Harris, R. K.; Holstein, P.; Reinsberg, S. A.; Yamauchi, K. *Polymer* **2001**, *42*, 8137–8151.
(57) Ando, S.; Harris, R. K.; Reinsberg, S. A. *Magn. Reson. Chem.* **2002**, *40*, 97–106.

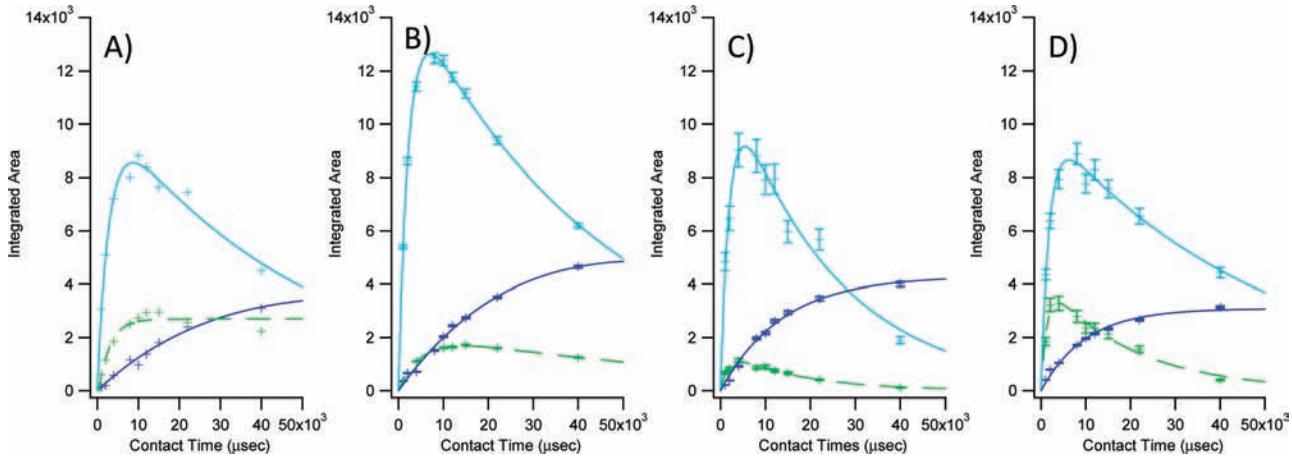

Figure 4. ^{77}Se{^{1}H} CP-MAS build up curves for (A) 3.1, (B) 4.3, (C) 6.1, and (E) 6.9 nm Cd^{77}Se QDs. The dark blue line represents the intensity of the core (peak 1) ^{77}Se sites, the light blue line represents surface (peak 2) ^{77}Se sites, and the green line represents the ligation layer (peak 3) for ^{77}Se bound to TOP. Contact times used to generate build up curve are 1, 2, 4, 8, 10, 12, 15, 22, and 40 ms.

Table 2. Time Constants for Cd^{77}Se QDs[a]

^{77}Se CP-MAS		sample 2 (3.1 nm)	sample 3 (4.3 nm)	sample 4 (6.1 nm)	sample 5 (6.9 nm)
peak 1 (core, blue)	T^*_{HSe} (ms)	28.5 ± 5.7	22.6 ± 2.5	13.7 ± 1.2	9.9 ± 0.9
	$T^*_{1\rho H}$ (ms)	–	–	–	–
peak 2 (surface, teal)	T^*_{HSe} (ms)	2.9 ± 0.3	2.2 ± 0.1	2.0 ± 0.3	1.7 ± 0.3
	$T^*_{1\rho H}$ (ms)	48.7 ± 7.1	43.6 ± 1.4	23.5 ± 3.4	49.3 ± 5.2
peak 3 (TOP−^{77}Se, green)	T^*_{HSe} (ms)	5.0 ± 0.5	5.1 ± 0.2	1.7 ± 0.3	1.3 ± 0.2
	$T^*_{1\rho H}$ (ms)	75.8 ± 14.5	67.9 ± 3.9	16.7 ± 2.3	19.6 ± 2.7
^{1}H spin lock	$T_{1\rho H}$ (ms)	83.1 ± 0.9	21.52 ± 0.7	28.36 ± 0.5	31.9 ± 0.6
	$T_{1\rho H}$ (ms)	19.3 ± 0.6	7.7 ± 0.2	9.06 ± 0.5	9.3 ± 0.3
calculated by overall integration of ^{77}Se CP-MAS intensities	T^*_{HSe} (ms)	3.1 ± 0.2	2.1 ± 0.1	1.7 ± 0.2	1.3 ± 0.1

[a] The dash (−) indicates the $T^*_{1\rho H}$ for the core signals are too long to be measured in the experimental time frame.

observation indicates ^{77}Se is likely only polarized by a small subpopulation of ^{1}H on the surface. Inspection of the direct pulse MAS measurement for the ^{31}P data for the QDs with size (Supporting Information Figure 4) confirms this assumption since two distinct ^{31}P species are observed, TOP and TOPO. Analyzing the total integrated area between the two regions suggests that the percentages of TOP bound to Se, TOP to Cd, and TOPO in the samples are unfortunately not uniform across the QD samples and require further investigation into the reaction conditions (temperature, time, reactants) and size-dependent changes to the observed surface passivation. This is also apparent in the ^{1}H NMR under high spinning speed (24 kHz), showing that multiple sites are present (Supporting Information Figure 5). Although this does not eliminate the possibility of changes in the ligand packing modulating the degree of reconstruction, it is also possible that as the QD grows changes to specific features[32] (edge, vertex) on the surface of the QD may result in the observed discontinuity in TOP−^{77}Se T^*_{HSe} and $T^*_{1\rho H}$ with QD size. The change in ligand packing at the QD surface could potentially impact the cross-polarization behavior for this size domain; however, it is not possible to definitively support this observation based on the NMR results alone.

To ensure the values for T^*_{HSe} (build-up time constant) and $T^*_{1\rho H}$ (decay time constant are not misinterpreted in CP-MAS experiments), the value of $T_{1\rho H}$ must be independently measured using a ^{1}H detected spin lock experiment to validate the assignments from CP-MAS.[58] In Supporting Information Figure 5 the ^{1}H spin-lock experiment on the Cd^{77}Se QDs exhibits multiple ^{1}H contributions attributable to different ^{1}H subpopulations with mobility differences. While ^{1}H spectra lack the resolution necessary for making assignments, different ^{1}H sites include positions along the alkane chain or TOP passivants on potentially different QD faces. The measured $T_{1\rho H}$ and $T^*_{1\rho H}$ correlate best for ^{77}Se{^{1}H} CP-MAS signal from TOP−^{77}Se; we consider this result reasonable because these ^{77}Se atoms are most strongly coupled to ^{1}H. These values are much longer than the values assigned to T^*_{HSe}, confirming the validity of the assignments. We were not able to obtain good fits to the TOP−^{77}Se CPMAS buildup data using the directly measured ^{1}H $T_{1\rho H}$ values, indicating that different ^{1}H sites transfer polarizations to ^{77}Se with different degrees of efficiency. Since surface and core regions correspond to ^{77}Se that is not directly coupled to ^{1}H, we believe the larger observed $T^*_{1\rho H}$ are subject to spin diffusion effects.

Spin Diffusion. The measured T^*_{HSe} values in Table 2 are observed to depend on both depths within a QD and overall QD size. A plot of the T^*_{HSe} data versus size for the surface, core, and total integrated NMR intensity exhibits a linear decrease with increasing size (Figure 5). It should be noted that the total T^*_{HSe} was determined by fitting the rise of total integrated ^{77}Se intensity from Figure 2 for CP contact times up to the peak intensity in each build-up curve. Since CP-MAS measurements are dominated by short-range contacts, the value for T^*_{HSe} most likely reflects spin diffusion from the surface layers into the core of the QD. The observed linear decrease with size is suggestive of a diffusion problem within the QD,

(58) Klur, I.; Jacquinot, J. F.; Brunet, F.; Charpentier, T.; Virlet, J.; Schneider, C.; Tekely, P. *J. Phys. Chem. B* **2000**, *104*, 10162–10167.

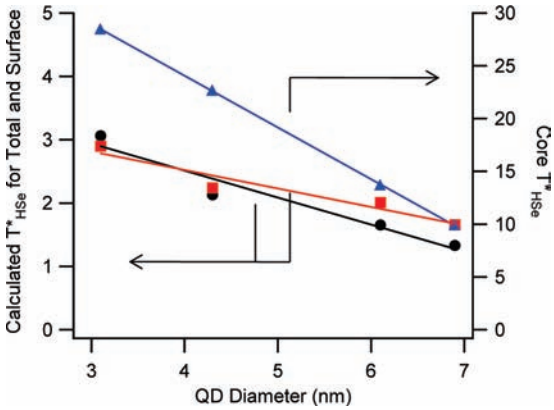

Figure 5. T^*_{HSe} for surface (red), core (blue), and total (black) ^{77}Se vs QD diameter. Solid curves are best fit lines.

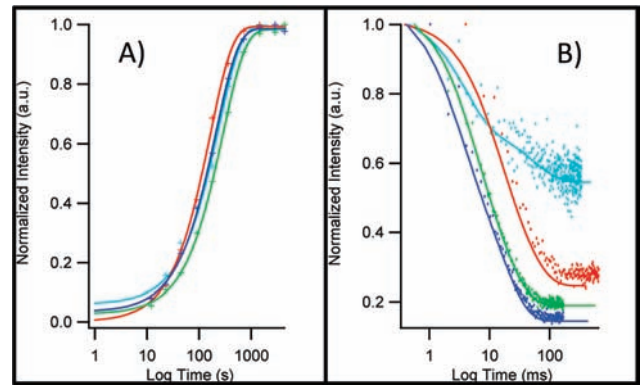

Figure 6. Size-dependent (A) T_1 and (B) T_2 data for Cd^{77}Se: 3.1 nm = light blue, 4.3 nm = red, 6.1 nm = green, 6.9 nm = dark blue. The data is fit to a single-exponential function for T_1 and biexponential function for T_2.

which would be expected to be important given the QD size-dependent surface curvature and surface-to-volume ratio. Unfortunately, a purely geometric approach to describing the T^*_{HSe} data in terms of spin diffusion as a function of QD size as described by a Fick's Law diffusion analysis (Supporting Information) in which the QD core is assumed to be represented by spherical symmetry and uniform spin diffusivity is not capable of explaining the QD size trends in Figure 5. Fick's model predicts an *increase* rather than the observed *decrease* in T^*_{HSe} for the total integrated signal as the QD increases in size. Possible explanations of the observed behavior can be described in terms of a breakdown of assumptions underlying the spin transport model, which assumes spin diffusion is not influenced by the interfaces that arise in a QD and more importantly will be size dependent. Chemical shift differences between the surface and the core ^{77}Se signal suggest that the surface layer has a different structure from the core and that spin diffusivity should vary between sublayers. The surface layer could be a diffusional barrier with decreasing thickness as QDs grow indicative of a size-dependent reconstruction in the outer layers of a Cd^{77}Se QD. Size-dependent surface properties may also play a role since shorter T^*_{HSe} for larger QD samples could be explained in terms of increased ligand coverage, ligand packing differences on the QD facets, and decreased ligand dynamics.[21] Although ^{1}H−^{77}Se cross-polarization at the surface is the ultimate source of signal, as explained in the Supporting Information the observed size dependence of T^*_{HSe} for the TOP−^{77}Se does not explain the QD size dependence of the T^*_{HSe} in the deeper layer under the simplified spin diffusion model.

T_2 Spin-Relaxation Dynamics. The measurement of transverse spin relaxation rates in the Cd^{77}Se QD is complicated by the presence of dipole−dipole coupling, structural interfaces, and the near unity isotopic enrichment of the ^{77}Se sites, although homonuclear coupling effects are attenuated by MAS. Dipole−dipole coupling in semiconductors has recently attracted much attention due to the differences in reported T_2 values when measured by CPMG (Carr−Purcell−Meiboom− Gill) and Hahn−echo approaches.[38,39,43,52,59] The recent studies on semiconductors have indicated that complex spin relaxation pathways in semiconductors, including Si, Ge, and Y_2O_3, may give rise to a biexponential decay for a CPMG-measured process in which the long T_2 relaxation has been attributed to dipole−dipole coupling. The exact nature of the biexponential relaxation in the CPMG results is still under discussion.[52]

The T_1 and T_2 spin-relaxation data were measured for the total sample without attempting to deconvulute the contributions of specific sites. Although the measurement of T_1 and T_2 for individual components would be ideal, unfortunately these experiments are cost prohibitive and difficult to assess due to overlapping signals. The ensemble-averaged T_1 and T_2 signals were measured by saturation recovery−CPMG techniques[60,61] (Figure 6 and summarized in Table 1). In all cases the T_1 is fit to a single-exponential decay while the T_2 is fit to a biexponential decay. The experimental results for the CdSe QDs indicate that only a small size dependence in T_1 values (160−286 s) is observed; however, larger changes in the long time component of T_2 decay occur with size. The fast T_2 component does not follow any obvious size dependence; 4.3 nm sample seems to be an outlier. It is worth noting that the size range is reminiscent of the discontinuity that occurs for ligand packing on CdSe,[21] elastic modulus changes,[14] and the measured $T_{1\rho H}$ data. We speculate this may suggest this QD size may be structurally and electronically unique; further studies are underway. The slower T_2 decay component decreases from $T_{2,1}$ = 61 (2.9 nm) to $T_{2,2}$ = 16 ms (6.9 nm).

Changes in Bonding. Changes in the structural and associated electronic environments in QDs will impact the chemical bonding.[25,26,44] X-ray diffraction has shown the Se atoms in the core of the CdSe QD exist largely in chemically similar tetrahedral environments, while the surface sites exist in distorted sites due to surface ligation and dangling bonds. Recent experimental results on core and core−shell QDs indicate the structural changes may be more complex with depth-dependent localized changes in the lattice.[15,17,20] Interrogation of the NMR spectra provide direct insight into the size-dependent changes in atomic disorder and local chemical potential changes occurring around the Se atoms as a function of size by analysis of the chemical shift anisotropy.

The expected change in the chemical shift for the Se sites as a function of size can be rationalized by considering the implication of changes in bonding around the Se atom through the use of the Ramsey expression.[62,2,31] The Ramsey expres-

(59) Li, D.; Dementyev, A. E.; Dong, Y.; Ramos, R. G.; Barrett, S. E. *Phys. Rev. Lett.* **2007**, *98*, 190401.
(60) Carr, H. Y.; Purcell, E. M. *Phys. Rev.* **1954**, *94*, 630–638.
(61) Meiboom, S.; Gill, D. *Rev. Sci. Instrum.* **1958**, *29*, 688–691.

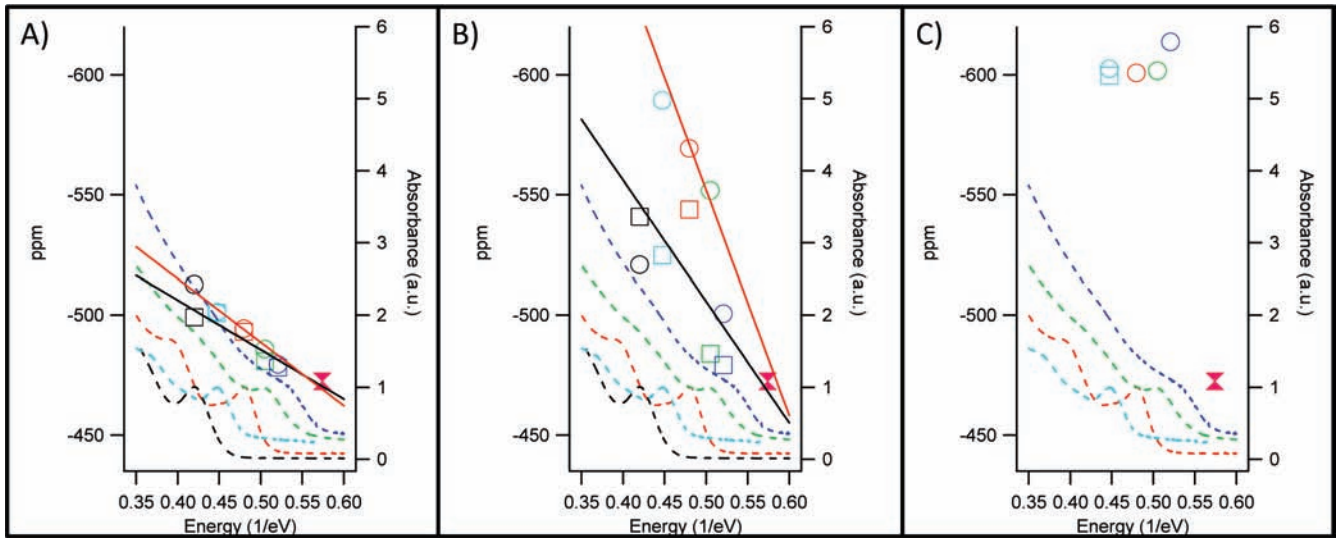

Figure 7. Ramsey plot of chemical shift (ppm) and absorbance with respect to inverse band-gap energy (1/eV) for Cd^{77}Se QD samples (2.9 (black), 3.1 (light blue), 4.3 (red), 6.1 (green), and 6.9 nm (dark blue)). Pink hourglass represents bulk CdSe within all three plots: (A) core ^{77}Se sites, (B) near-surface and surface ^{77}Se sites, (C) surface ^{77}Se sites bound to TOP; (○) CP-MAS assignments and (□) spin−echo assignments.

sion relates σ_p^{iso} to the probability of an electron being in the excited state which can lead to less shielding and a more positive chemical shift. The paramagnetic term is defined as

$$\sigma_p^{iso} = -\frac{\mu_0 e^2 \hbar^2}{8m_e^2 \pi} \sum_{n\neq 0} \frac{1}{\Delta E_n} \left[\left\langle 0 \left| \sum \frac{\delta}{l \delta \phi_l} \right| n \right\rangle \times \left\langle n \left| \sum \frac{\delta}{l' \delta \phi_{l'}} \frac{1}{q_{l'}^3} \right| 0 \right\rangle + \left\langle 0 \left| \sum \frac{\delta}{l' \delta \phi_{l'}} \frac{1}{q_{l'}^3} \right| n \right\rangle \times \left\langle n \left| \sum \frac{\delta}{l \delta \phi_l} \right| 0 \right\rangle \right] \quad (4)$$

where μ_0 is the permittivity of vacuum, e is the charge of an electron, $\hbar$ is Planck's constant divided by 2π, m is the mass of an electron, φ_l is the angular momentum operator which is the change in l with respect to the magnetic field, and q_l is the distance between two dipoles. ΔE_n in the equation is the energy separation between the ground state, $|0\rangle$, and nth excited state, $|n\rangle$,which scales with the band gap (E_g) in a semiconductor.[2,31,62]

A plot of the chemical shift for the core (Figure 7A), surface (Figure 7B), and TOP−^{77}Se (Figure 7C) resonances versus the inverse band-gap energy are in agreement with the Ramsey expression, but the differences between the specific sites are informative. The spin−echo and CP-MAS exhibit different slopes for the data but the same trend for the core and surface resonances. The NMR resonances for the core and surface terms exhibit a shift to a more positive value with increasing size (decreasing bandgap) with the core component exhibiting a shallower slope than the surface term. The observed linear shift in the core and surface with size suggests that the ^{77}Se sites are more shielded as the QD size decreases, particularly at the surface sites. The TOP−^{77}Se signal exhibits no significant change in chemical shift. The lack of an observed shift for TOP−^{77}Se is not surprising, as the ligation of the surface is expected to be largely insensitive to changes in the QD structure as the bonding interaction between Se and phosphorus is dominated by *d*-back-bonding interactions. The shift in frequency with size for the core component is consistent with the early reports correlating the Ramsey equation-predicted shift with band-gap energy in QDs.[2,31]

The strongest evidence of the observed "Ramsey-like" behavior for the NMR chemical shift and the QD size can be generated by plotting the chemical shift change with respect to the effective mass approximation, commonly referred to as the "Brus" equation. It can be shown that the chemical shift, $\Delta\nu(\nu_{bulk} - \nu_{QD})$, is inversely proportional to ΔE_g, (E_g(bulk) − E_g(QD)) based on the Ramsey expression.[63] Thus, one may write an expression linking $\Delta\nu$ to the size-dependent effective mass approximation such that

$$\frac{1}{\Delta\nu} = \frac{ad^2 + bd + c}{d^2} \quad (5)$$

where d is the radius of the QD, c is an empirical constant for the confinement term, b is a constant for the Coulomb term, and a is a correction term.[64] The fit of eq 5 is shown in Figure 8, indicating good agreement between the observed chemical shift and the observed optical transition for the first exciton ($1S_{3/2} \rightarrow 1S_e$) in the CdSe QD. The ratio of the confinement to Coulomb term is consistent for the spin−echo and CP-MAS experimental fits (~1.2 (core) and ~1.1 (surface)) and more importantly are similar to the ratio extracted from the optical experiment (1.5), implying the observed correlation of NMR and EMA is meaningful.

The results confirm the NMR-measured core and surface signatures represent independent sites that are uniquely coupled to changes in the internal electronic properties of the QD, and thus, the size-dependent correlation of the NMR shifts to the Ramsey expression and the effective mass approximation have implications with respect to the orbital hybridization for the Se atoms within the QD. To rationalize the slope difference in Figure 7 between the core and the surface, a model to explain the observed chemical shift difference based on changes in the electron orbital hybridization for a Se atom in a tetrahedral site

(62) Ramsey, N. F. *Phys. Rev.* **1950**, *78*, 699–703.
(63) Brus, L. E. *J. Chem. Phys.* **1984**, *80*, 4403–4409.
(64) Swafford, L. A.; Weigand, L. A.; Bowers, M. J.; McBride, J. R.; Rapaport, J. L.; Watt, T. L.; Dixit, S. K.; Feldman, L. C.; Rosenthal, S. J. *J. Am. Chem. Soc.* **2006**, *128*, 12299–12306.

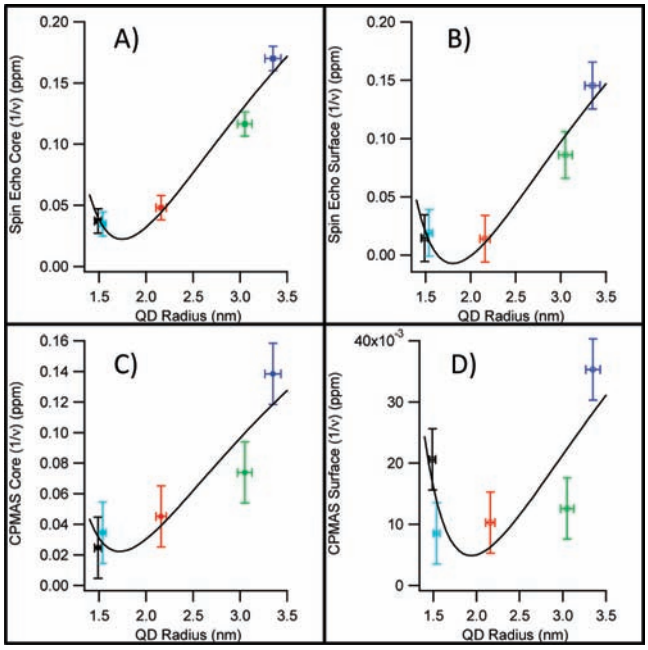

Figure 8. Spin−echo and CP-MAS (contact time = 12 ms) ^{77}Se NMR data illustrating the change in chemical shift vs QD size: (A) spin−echo core, (B) spin−echo surface, (C) CP-MAS core, and (D) CP-MAS surface sites. Cd^{77}Se QD samples: 2.9 (black), 3.1 (light blue), 4.3 (red), 6.1 (green), and 6.9 nm (dark blue).

is useful. The bonding for the Se atom is dominated by a mixture of *s*-, *p*-, and to a partial extent *d*-orbital overlap with Cd. Of these the valence band for CdSe is largely dominated by the Se *p*-orbital character. Using a simple hybridization model to assess the bonding for a Se atom in tetrahedral symmetry, the σ-bonding interaction can be approximated as 0.25 *s*-orbital character and 0.75 *p*-orbital character per bond. As the tetrahedral symmetry is reduced by trigonal or tetragonal distortion, the bonding will exhibit an increase in the *s* character. An increase in *s* character would result in an increase in electron density at the nuclei and thus a resonance with a more negative chemical shift. X-ray absorption spectroscopy analysis[65] of CdSe QDs supports the conclusion of increasing *s* character is with decreasing QD size. While the XAS methods cannot distinguish between core and surface atoms, it is reasonable to believe the logic is transferrable and an increasing *s* character in the conduction band (Cd-based orbital) is consistent with the increased surface to core contribution to decreasing size. The results are consistent with the NMR results from Chmelka et al. on ZnSe postulated electronic changes in the QD based on density functional theory predictions.[44]

A more quantitative analysis of this simple model is provided by further interpreting the Ramsey expression in terms of the orbital overlap model since σ_p is dominated by the 4_p electrons on Se

$$\sigma_p \approx \langle r^{-3} \rangle_{4p} \cdot \Delta E^{-1} \cdot \sum Q \qquad (6)$$

where $\langle r^{-3} \rangle_{4p}$ is the inverse cube of the radius of the 4_p electrons (orbital extension), ΔE^{-1} is the mean excitation energy, which is correlated to the band-gap energy in semiconductors, and ΣQ is the charge-density−bond order matrix.[62,66] While it is difficult to independently interpret the three factors since $\langle r^{-3} \rangle_{4p}$ and ΣQ are closely connected, the trend in the data can be interpreted for the core versus surface by invoking changes in the respective orbital character. For a given size if the symmetry is reduced from a pure T_d site at the surface, the *s* character in the bond increases while the *p* character decreases, in effect reducing the bonding interaction (ΣQ) between the *p* orbital on the Se and the Cd, resulting in a smaller value for σ_p and thus a more negative chemical shift for the surface resonances. The over-simplified angular orbital overlap model correlates well with the observations from the Ramsey plot (Figure 7). Thus, the QD can be envisioned as consisting of core layers with undistorted tetrahedral symmetry sites and a self-terminated outer shell that experiences reconstruction (Figure 1). The differences in chemical environment lead to the experimental observation that the core ^{77}Se resonances are shifted to a more positive chemical shift relative to the surface (outer shell layers) Se atoms. Physically the results most likely reflect a combination of changes in the lattice strain arising from broken symmetry due to ligation of the surface, reconstruction of unligated sites (dangling bonds), and contributions from ligand-induced compression. Interpreting the observed chemical shift with size implies a decrease in the orbital overlap for both core and surface occurs as the QD grows. From a bonding perspective this could be interpreted as a decrease in the covalent character of the bond as the QD increases in size. Such a change is reasonable as bulk CdSe is better described as an ionic semiconductor while a cluster of CdSe atoms is better described as a coordination-type complex with greater covalent character.

Conclusions

The NMR results strongly support a model in which Cd^{77}Se QDs contain core and surface regions. For QDs with diameters less than 4 nm, reconstruction seems to be more global (Figure 1C), effecting both surface and core signals. Cd^{77}Se QDs greater than 4 nm in diameter are better modeled by a strongly localized, surface-truncated model (Figure 1D) in which reconstruction is limited to the surface region. Trends measured by NMR support the interpretation that reconstruction is more extreme for small QDs, supporting previous claims that QDs undergo surface reconstruction to relieve the stress created due to truncation of the high-energy surface planes. Analysis of direct polarization and ^{77}Se CP-MAS NMR indicates that surface layer thickness and ligand surface coverage depend on QD size due to surface reconstruction. Sublayer ^{77}Se is polarized in a CP-MAS experiment by ^{77}Se spin diffusion through isotopically enriched lattices, though polarization transport in spherical geometry alone is not enough to explain observed size dependences of observed relaxation and polarization transfer rates.

The precise ^{77}Se NMR peak shifts can be correlated with size-dependent core and surface site contributions. The different observed slopes for the core and surface chemical shifts from the Ramsey equation suggest that a unique depth-dependent bonding character exists in the QD. Valence bond theory arguments coupled to the Ramsey expression and EMA imply the highly distorted surface leads to greater s character than the core, implying the bonding is distorted from T_d to a trigonal or tetragonal symmetry in the outer shell of the QD. The increase in s character for these distorted surface sites result in further shielding of the nuclei, and thus, the observed chemical shift is a more negative value.

(65) Lee, J. R. I.; Meulenberg, R. W.; Hanif, K. M.; Mattoussi, H.; Klepeis, J. E.; Terminello, L. J.; van Buuren, T. *Phys. Rev. Lett.* **2007**, *98*, 4.
(66) Duddeck, H. *Prog. Nucl. Magn. Reson. Spectrosc.* **1995**, *27*, 1–323.

Acknowledgment. We wish to thank NSF-CHE-0911080 and NSF-DMR-0701462 for support of the research. The TEM facility is supported by National High Magnetic Field Laboratory under NSF DMR-0084173 and the state of Florida. We would like to acknowledge Dr. Tom Gedris for his assistance and discussions. We would like to acknowledge Dr. Mia Berrettini for initial studies on the solid-state NMR for CdSe.

Supporting Information Available: NMR pulse sequence for saturation recovery−CPMG experiments, overlay of ^{77}Se CPMG and spin-echo measurements, QD characterization data (UV−vis, XRD, and TEM),^{31}P MAS direct pulse NMR for the CdSe QDs, and ^{1}H spin lock measurement as high spinning speed; in addition, the theory and discussion of anticipated QD size effects on QD size based on spin diffusion and information describing the calculation of core and surface atom numbers using Crystal Maker and Excel has been provided. This material is available free of charge via the Internet at http://pubs.acs.org.

JA907511R